Metamorphism during temperature gradient with undersaturated advective airflow in a snow sample

Pirmin Philipp Ebner[1,2], Martin Schneebeli[2,*], and Aldo Steinfeld[1]

[1] *Department of Mechanical and Process Engineering, ETH Zurich, 8092 Zurich, Switzerland*

[2] *WSL Institute for Snow and Avalanche Research SLF, 7260 Davos-Dorf, Switzerland*

Abstract

Snow at or close to the surface commonly undergoes temperature gradient metamorphism under advective flow, which alters its microstructure and physical properties. Time-lapse X-ray micro-tomography is applied to investigate the structural dynamics of temperature gradient snow metamorphism exposed to an advective airflow in controlled laboratory conditions. Cold saturated air at the inlet was blown into the snow samples and warmed up while flowing across the sample with a temperature gradient of around 50 K m^{-1}. Changes of the porous ice structure were observed at mid-height of the snow sample. Sublimation occurred due to the slight undersaturation of the incoming air into the warmer ice matrix. Diffusion of water vapor opposite to the direction of the temperature gradient counteracted the mass transport of advection. Therefore, the total net ice change was negligible leading to a constant porosity profile. However, the strong recrystallization of water molecules in snow may impact its isotopic or chemical content.

Keywords: snow, temperature gradient, metamorphism, advection, sublimation, tomography

[*] Corresponding author. Email: schneebeli@slf.ch,

1. Introduction

Snow has a complex porous microstructure and consists of a continuous ice structure made of grains connected by bonds and inter-connecting pores (Löwe et al., 2011). It has a high permeability (Calonne et al, 2012, Zermatten et al., 2014) and under appropriate conditions airflow through the snow structure can occur (Sturm and Johnson, 1991) due to variation of surface pressure (Colbeck, 1989; Albert and Hardy, 1995), simultaneous warming and cooling, and induced temperature gradients (Sturm and Johnson, 1991). Both diffusive and advective airflows affect heat and mass transport in the snowpack and influence chemical concentrations (Gjessing, 1977; Waddington et al., 1996). Various airflow conditions in a snow sample occur, namely: isothermal airflow, air cooling by a negative temperature gradient along the airflow leading to a local supersaturation of the air, and air warming by a positive temperature gradient along the airflow leading to a local undersaturation of the air (Fig. 1). In general, in a natural snowpack close to the surface (< 1cm) two additional conditions can occur: (1) warm air enters a snowpack having a positive temperature gradient leading to a supersaturation of the air at the entrance, and (2) cold air enters a snowpack having a negative temperature gradient leading to an undersaturation of the air at the entrance. However, because snow has a high heat capacity compared to the air, a high specific surface area, and therefore a high convective heat transfer to the air, a "quasi" thermal equilibrium (the term "quasi" is used because normally the snow structure continuously changes and therefore the equilibrium conditions as well) is usually assumed inside the snowpack (> 1 cm). In this paper, only conditions deeper than > 1 cm inside a snowpack are considered. Under isothermal condition, the continuous sublimation and deposition of ice is due to higher vapor pressure over convex surfaces and lower vapor pressure over concave surfaces, respectively (Kelvin-effect) (Neumann et al., 2008; Ebner et al., 2014). However, applying a fully isothermal saturated airflow across a snow sample has been shown to have no influence on the coarsening rate that is typical for isothermal snow metamorphism independently of the transport regime in the pores at a physically possible Peclet-number (Ebner et al., 2015a). When applying a temperature gradient, the effect of sublimation and deposition in the snow results from interaction between snow temperature and the local relative humidity in the pores. If vapor is advected from a warmer zone into a colder zone, the air becomes supersaturated, and some water vapor deposits onto the surrounding ice grains. This leads to a change in the microstructure creating whisk-

er-like crystals (Ebner et al., 2015b). Whisker-like crystals are very small (~10-30 μm) elongated monocrystals. A flow rate dependence of the deposition rate of water vapor deposition at the ice interface was observed, asymptotically approaching an average estimated maximum volumetric deposition rate on the whole sample of $1.05 \cdot 10^{-4}$ kg m^{-3} s^{-1} (Ebner et al., 2015b). Contrarily, if the temperature gradient acts in the same direction of the airflow, the airflow through the snow brings cold and relatively dry air into a warmer area, causing that the pore space air becomes undersaturated, and surrounding ice sublimates. Here, we investigate specifically this last effect.

Sublimation of snow is a fundamental process that affects its crystal structure (Sturm and Benson, 1997), and thus is important for ice core interpretation (Stichler et al., 2001; Ekaykin et al., 2009), as well as calculation of surface energy balance (Box and Steffen, 2001) and mass balance (Déry and Yau, 2002). Kaempfer and Plapp (2009) suggest that condensation of water vapor will have a noticeable effect on the microstructure of snow using a 3D phase-field model, which is also confirmed by a two dimensional finite-element model using airflow velocities, vapor transport and sublimation rates of Albert (2002). Neumann et al. (2009) determined that there is no energy barrier to be overcome during sublimation, and suggest that snow sublimation is limited by vapor diffusion into pore space, rather than by sublimation at the crystal surface.

In the present work, we studied the surface dynamics of snow metamorphism under an induced temperature gradient and saturated airflow in controlled laboratory experiments. Cold saturated air at around -14 ºC was blown into the snow samples and warmed up to around -12.5 ºC while flowing across the sample. Sublimation of ice was analyzed by in-situ time-lapse experiment with microcomputer tomography (micro-CT) (Pinzer and Schneebeli, 2009; Chen and Baker, 2010; Pinzer et al., 2012; Wang and Baker, 2014; Ebner et al., 2014) to obtain the discrete-scale geometry of snow. By using discrete-scale geometry, all structures are resolved with a finite resolution corresponding to the voxel size of 18 μm.

2. Time-Lapse tomography experiments

Temperature gradient experiments with fully saturated airflow across snow samples (Ebner et al., 2014) were performed in a cooled micro-CT (Scanco Medical μ-CT80) in a cold laboratory temperature of T_{lab} = -14˚C. Cold saturated air was blown into the snow samples and warmed up while flowing across the sample. Aluminum foam including a heating wire was used to warm the side of the snow opposite to the entering air-

flow. We analyzed the following flow rates: a volume flow of 0 (no advection), 0.3, 1.0, and 3.0 liter/min. Higher flow rates were experimentally not possible as shear stresses by airflow destroyed the snow structure (Ebner et al., 2015a). Nature identical snow produced in a cold laboratory (Schleef et al., 2014) was used for the snow sample preparation (water temperature: 30 ºC; air temperature: −20 ºC). The snow was sieved with a mesh size of 1.4 mm into a box, and was sintered for 27 days at -5˚C to increase its strength. The sample holder (diameter: 53 mm; height: 30 mm) was filled by cutting out a cylinder from the sintered snow and pushing into the sample holder without mechanical disturbance of the core. The snow samples were measured with a voxel size of 18 μm^3 over 108 h with time-lapse micro-CT measurements taken every 3 h, producing a sequence of 37 images. The innermost 36.9 mm of the total 53 mm diameter were scanned, and subsamples with a dimension of 7.2 mm × 7.2 mm × 7.2 mm were extracted for further processing. The imaged volume was in the centre of the sample (Fig. 1 c)). A linear encoder with a resolution of less than 1 voxel (< 2 µm) was used to verify that the scans were taken at the same position. Additionally, a cross-correlation function was applied to supress all erroneous data from the dataset. The reconstructed micro-CT images were filtered by using a 3 × 3 × 3 median filter followed by a Gaussian filter (σ = 1.4, support = 3). The clustering-based Otsu method (Otsu, 1979) was used to automatically segment the grey-level images into ice and void phase. Morphological properties of the two-phase system were determined based on the geometry obtained by the micro-CT. The segmented data were used to calculate a triangulated ice matrix surface and tetrahedrons inscribed into the ice structure. Morphological parameters such as porosity (ε) and specific surface area (SSA) were then calculated of subsamples of the size of 6.3 mm × 6.3 mm × 6.3 mm samples. An opening-based morphological operation was applied to extract the mean pore size of each micro-CT scan (d_{mean}) (Haussener et al., 2012). As additional physical and structural parameter, the effective thermal conductivity k_{cond} was estimated by direct pore-level simulations (DPLS) to determine the influence of changing microstructure. DPLS determined the effective thermal conductivity by solving the governing steady-state heat conduction equations within the solid phase and the stagnant fluid phase (Kaempfer et al., 2005; Petrasch et al., 2008; Calonne et al., 2011; Löwe et al., 2013).

3. Results

Time-lapse tomographic scans were performed with temperature gradients between 43-53 K m^{-1} (Table 1). Small fluctuations of the measured inlet and outlet temperature were due to temperature regulation both inside the cold chamber and inside the micro-CT (Ebner et al., 2014). A shift of $\Delta t < 10$ min between inlet and outlet temperature indicated that a fast equilibrium between the temperature of the snow and the airflow was reached (Albert and Hardy, 1995; Ebner et al., 2015b). The morphological evolution was similar between all four experiments and only a slight rounding and coarsening was visually observed during the 108 h experiment (Fig. 2). The initial ice grains did not change with time and the locations of sublimation and deposition for "ota3" and "ota4" is shown in Fig. 3. Sublimation of 7.7 % and 7.6 % of the ice matrix and deposition of 6.0 % and 9.6 % on the ice matrix were observed. The data were extracted by superposition of vertical cross-sections at 0 and 108 hours with an uncertainty of 6%. The mass sublimated preferentially at locations of the ice matrix with low radii and was relocated leading to a smoothing of the ice surface and to an increase in the size of pores (Fig. 4 a)). The pore size (uncertainty ~6 %) increased by 3.4 %, 3.6 %, 5.4 % and 6.5 % for 'ota1', 'ota2', 'ota3', and 'ota4', respectively.

Loss of ice due to sublimation could not be detected by the micro-CT scans due to limited accuracy and no flow rate dependence was observed during any of the four experiments. The temporal evolution of the porosity, shown in Fig. 4 b), did not change with time and the influence of sublimation of water vapor was not observed. Only 'ota2' showed a slight drop in the temporal evolution of the porosity until 18 h into the experiment but kept constant afterwards. This slight drop (≈ 0.5 %) was probably caused by settling of the snow. Coarsening was observed for each experiment but the influence of changing airflow was not visible, confirmed by the temporal SSA evolution, shown in Fig. 4 c).

The repositioning of water molecules led to a smoothing of the ice grains, but did not affect the thermal conductivity of snow. This quantity (standard deviation ~0.025 W m^{-1}) slightly increased after applying airflow to the temperature gradient, shown in Fig. 4 d), but no flow rate dependence was observed. Every third scan was used to extract the thermal conductivity and a change of -2.6 %, 3.6 %, 2.2 %, and 2.7 % for 'ota1', 'ota2', 'ota3', and 'ota4' was detected.

5. Discussion

The rate of deposition onto the ice surface depends on the flow rate where warm saturated air cooled down while flowing through the sample, as shown in previous experiments (Ebner et al., 2015b). Its deposition rate asymptotically reached a maximum of $1.05 \cdot 10^{-4}$ kg m^{-3} s^{-1}. In this study, changing the temperature gradient leads to a warming up of a cold saturated flow, and resulted in a sublimation rate too small for the analyzed period of the experiment to measure a flow rate dependence by the micro-CT and an influence on the temporal density gradient.

A structural change of the ice grains and repositions of water molecules was observed but the total net flux of the snow was not affected. The superposition of a vertical cross-section in Fig. 3 shows a big effect on reposition of water molecules on the ice structure. However, the temporal porosity (Fig. 4 b) was not affected and the total water vapor net flux was negligible for the analyzed volume. Continued sublimation and deposition of water molecules due to the temperature gradient led to a saturation of the pore space. The vapour pressure of the air in the pore was in equilibrium with the water pressure of the ice, given by the local temperature. The entering air warmed up, allowing vapour sublimating from the snow sample to be incorporated into the airflow. As time passed, the snow grains in the sample became more rounded as convexities sublimated. As a result of the reduced curvature, the rate of sublimation decreased and less vapour was deposited in concavities and therefore the surface asperities persisted longer. Finally, the "Kelvin-effect" had a longer impact on the structural change of the ice grains and the reposition of water molecules. In addition, the uptake of water molecules and their transport due to warming during advection was counteracted by diffusion of water molecules due to the temperature gradient. As thermally induced diffusion was opposite to the airflow gradient, a backflow of water vapor occurred and the two opposite fluxes counteracted each other. The Peclet numbers ($Pe = u_D \cdot d_{mean}/D$, where D is the diffusion coefficient of water vapor in air), describing the ratio of mass transfer between diffusion and advection, measured during each experiment, showed that diffusion was still dominant (Table 1). Therefore, water molecules were diffused along the opposite direction to the temperature gradient and advected along the flow direction leading to a back and forth transport of water molecules.

As a Peclet higher than 1 is not possible in natural snow (Ebner et al., 2015a), advection of cold saturated air into a slightly warmer snowpack has a significant influence not on the total net mass change but on the structural change of the ice grains due to re-

distribution of water vapour on the ice matrix. Also the increasing pore size has an influence on the flow field leading to a deceleration of the flow and therefore the interaction of an air-parcel with the ice matrix in the pores increases due to higher residence time. In addition, the diffusive transport rises whereas the advective transport decreases, changing the mass transport in the pores. Our results support the hypothesis of Neumann et al. (2009) that sublimation is limited by vapor diffusion into the pore space or kinetics effects (reaction effect) at crystal faces. This is supported by the temporal evolution of the porosity (Fig. 4 b)) and the SSA (Fig. 4 c)), as no velocity dependence was observed and the structural changes were too small to be detected by the micro-CT.

The influence of diffusion of water vapor in the direction of the temperature gradient and the influence of the residence time of an air-parcel in the pores were also confirmed by a low mass change at the ice-air interface. Overlapping two consecutive 3D images, the order of magnitude of freshly sublimated ice was detected. The absolute mass change at the ice-air interface (kg m^{-3} s^{-1}) estimated by the experimental results is defined as

$$S_{\mathrm{m,exp}} = \left| \rho_{\mathrm{i}} \frac{\Delta(1-\varepsilon)}{\Delta t} \right| \tag{1}$$

where $\Delta(1\text{-}\varepsilon)$ is the change in the porosity between two images separated by the time step Δt, and ρ_{i} is the density of ice. Albert and McGilvary (1992) and Neumann et al. (2009) presented a model to calculate sublimation rates directly in an aggregate snow sample

$$S_{\mathrm{m}} = \left| h_{\mathrm{m}} \mathrm{SA_V} (\rho_{\mathrm{sat}} - \rho_{\mathrm{v}}) \right| \tag{2}$$

where $\mathrm{SA_V}$ is the specific surface area per volume of snow, and h_{m} is the mass-transfer coefficient (m s^{-1}) given by Neumann et al., (2009)

$$h_{\mathrm{m}} = (0.566 \cdot \mathrm{Re} + 0.075) \cdot 10^{-3} \tag{3}$$

assuming that the sublimation occurs within the first few mm of the sample. Re (Re = $u_{\mathrm{D}} \cdot d_{\mathrm{mean}} / \nu$ where ν is the kinematic viscosity of the air) is the corresponding Reynolds-number of the flow. The absolute sublimation rate is driven by the difference between the local vapor density (ρ_{v}) and the saturation vapor density (ρ_{sat}) (Neumann et al., 2009; Thorpe and Mason, 1966). Table 2 shows the estimated absolute sublimation rate by the experiment (Eq. (1)) and the model (Eq. (2)). The very small change in porosity due to densification during the first 18 h for 'ota2' was not taken into account. The estimated sublimation rates by the experiment were two orders of magnitude lower than the mod-

eled values and also two orders of magnitude lower than during a negative temperature gradient along an airflow experiment (Ebner et al., 2015b). As the air in the pore space is always saturated (Neumann et al., 2009), the back diffusion of water vapor in the opposite direction of the temperature gradient led to a lower mass transfer rate of sublimation. The flow rate dependence for the model described is shown by the mass-transfer coefficient (Eq. 3), increasing with higher airflow. However, the values calculated from the experiment showed a different trend. Increasing the flow rate led to a lower mass transfer rate due to a lower residence time of the air in the pores. Transfer of heat toward and water vapor away from the sublimating interface may also limit the sublimation rate. In general, the results of the model by Neumann et al. (2009) have to be interpreted with care, as his model was set up to saturate dry air under isothermal conditions. Ice crystals sublimated as dry air enters the snow sample; water vapor was advected throughout the pore space by airflow until saturation vapor pressure was reached, preventing further sublimation. The model by Neumann et al. (2009) does not consider the influence of a temperature gradient and the additional vapor pressure gradient. However, our results concluded that a positive temperature gradient along the airflow has a significant impact on the sublimation rate, decreasing the rate by two orders of magnitude.

In the experiments by Neumann et al. (2009), sublimation of snow using dry air under isothermal condition showed a temperature drop for approximately the first 15 min after sublimation started and stayed constant because the latent heat absorption of sublimation for a given flow rate and heat exchange with the sample chamber equalized each other. Such a temperature drop was not observed in our experiments. In the experiments by Neumann et al. (2009) the amount of energy used for sublimation was between -10 and -40 J min^{-1} for saturation of dry air. Using the expected mass change at the ice-air interface $S_{m,exp}$ (Eq. (1)) and the latent heat of sublimation ($L_{sub} \approx 2834.1 \cdot 10^3$ J kg^{-1}) the energy needed for sublimation ranged between -2 and -12 J min^{-1} for our experiments. Our estimated values are a factor up to five lower than the estimated numbers of Neumann et al. (2009), because the entering air was already saturated (with reference to the cold temperature) at the inlet. The needed energy for sublimation could be balanced between the sensible heat carried into and out of the sample, and the exchange of the snow sample with the air stream and the surrounding prevented a temperature drop.

Thermal conductivity changed insignificantly in these experiments, especially for 'ota 1'. This indicates that air warming by a positive temperature gradient along the air-flow and an open system reduces or suppresses the increase in thermal conductivity usually observed by temperature gradient metamorphism (Loewe et al., 2013; Calonne et al., 2014), also the timescales are quite different between experiments. Compared to closed temperature gradient experiment, the applied temperature gradient induced an air movement and therefore reduced the impact on the snow metamorphism and its thermal conductivity, at least on the short term. As a recall, the thermal conductivity has been numerically estimated from the geometrical information of the sample only and no air movement was taken into consideration.

6. Summary and conclusion

We performed four experiments of temperature-gradient metamorphism of snow under saturated advective airflow during 108 h. Cold saturated air was blown into the snow samples and warmed up while flowing across the sample. The temperature gradient varied between 43 and 53 K m^{-1} and the snow microstructure was observed by X-ray micro-tomography every 3 h. The micro-CT scans were segmented, and porosity, specific surface area, and the mean pore-size were calculated. Effective thermal conductivity was calculated in direct pore-level simulations (DPLS).

Compared to deposition (shown in Ebner et al., 2015b), sublimation showed a small effect on the structural change of the ice matrix. A change in the pore size was most likely due to sublimation of ice crystals with small radii but a significant loss of water molecules of the snow sample and mass transfer away from the ice interface due to sublimation and advective transport could not be detected by the micro-CT scans and no flow rate dependence was observed. The interaction of mass transport of advection and diffusion of water vapor in the opposite direction of the temperature gradient and the influence of the residence time of an air-parcel in the pores led to a negligible total mass change of the ice. However, a strong reposition of water molecules on the ice grains was observed.

The energy needed for sublimation was too low to see a significant temperature drop because the needed energy was balanced between the sensible heat carried into and out of the sample, and the exchange of the snow sample with the air stream and the surrounding.

This is the third paper of a series analyzing an advective airflow in a snowpack in depth of more than 1 cm. Previous work showed that: (1) under isothermal conditions, the Kelvin-effect leads to a saturation of the pore space in the snow but did not affect the structural change (Ebner et al., 2015a); (2) applying a negative temperature gradient along the flow direction leads to a change in the microstructure and creation of whisker-like structures due to deposition of water molecules on the ice matrix (Ebner et al., 2015b); and (3) a positive temperature gradient along the flow had a negligible total mass change of the ice but a strong reposition effect of water molecules on the ice grains, shown in this paper. Conditions (1) and (3) showed that they have a negligible effect on the porosity evolution of the ice matrix except when sitting is concerned. Porosity changes can be neglected to improve models for snow compaction and evolution at the surface, however, mechanical processes like compaction strongly impact porosity. In contrast, conditions (2) showed a significant impact on the structural evolution and seems to be essential for such snowpack models and other numerical simulations. Nevertheless, the strong reposition of water molecules on the ice grains observed for all conditions (1) – (3) can have a significant impact on atmospheric chemistry and isotopic changes in snow.

Acknowledgements

The Swiss National Science Foundation granted financial support under project Nr. 200020-146540. The authors thank the reviewers E. A. Podolskiy and F. Flin for the constructive reviews and M. Jaggi, S. Grimm, H. Löwe for technical and modelling support.

References

Albert, M. R.: Effects of snow and firn ventilation on sublimation rates, Annals of Glaciology, 35, 52-56, 2002.

Albert, M. R. and Hardy, J. P.: Ventilation experiments in a seasonal snow cover, in Biogeochemistry of Seasonally Snow-Covered Catchments, IAHS Publ. 228, edited by K. A. Tonnessen, M. W. Williams, and M. Tranter, 41 –49, IAHS Press, Wallingford, UK, 1995.

Albert, M. R. and McGilvary, W. R.: Thermal effects due to air flow and vapor transport in dry snow, Journal of Glaciology, 38, 273-281, 1992.

Box, J. E. and Steffen, K.: Sublimation on the Greenland ice sheet from automated weather station observations, Journal of Geophysical Research, 107, 33965-33981, 2001.

Calonne, N, Flin, F., Morin, S., Lesaffre, B., and Rolland du Roscoat, S.: Numerical and experimental investigations of the effective thermal conductivity of snow, Geophysical Research Letter, 38, 1-6, 2011.

Calonne, N., Geindreau, C., Flin, F., Morin, S., Lesaffre, B., Rolland du Roscoat, S., and Charrier, P.: 3-D image-based numerical computations of snow permeability: links to specific surface area, density, and microstructural anisotropy, The Cryosphere, 6, 939-951, 2012.

Calonne, N., Flin, F., Geindreau, C., Lesaffre, B. and Rolland du Roscoat, S.: Study of a temperature gradient metamorphism of snow from 3-D images: time evolution of microstructures, physical properties and their associated anisotropy, The Cryosphere, 8, 2255-2274, 2014.

Chen, S., and Baker, I.: Evolution of individual snowflakes during metamorphism, Journal of Geophysical Research, 115, 1–9, 2010.

Colbeck, S. C.: Air movement in snow due to windpumping, Journal of Glaciology, 35, 209–213, 1989.

Déry, S. J. and Yau, M. K.: Large-scale mass balance effects of blowing snow and surface sublimation, Journal of Geophysical Research, 107, doi:10.1029/2001JD001251, 2002.

Ebner, P. P., Grimm, S., Schneebeli, M., and Steinfeld, A.: An instrumented sample holder for time-lapse micro-tomography measurements of snow under advective conditions, Geoscientific Instrumentation Methods and Data Systems, 3, 179–185, 2014.

Ebner, P. P, Schneebeli, M., and Steinfeld, A.: Tomography-based observation of isothermal snow metamorphism under advective conditions, The Cryosphere, 9, 1363–1371, 2015a.

Ebner, P. P, Andreoli, C., Schneebeli, M., and Steinfeld, A.: Tomography-based observation of ice-air interface dynamics of temperature gradient snow metamorphism under advective conditions, Journal of Geophysical Research, submitted, 2015b.

Ekaykin, A. A., Hondoh, T., Lipenkov, V. Y., and A. Miyamoto: Post-depositional changes in snow isotope content: preliminary results of laboratory experiments, Clim. Past Discuss., 5, 2239–2267, 2009.

354 Gjessing, Y. T.: The filtering effect of snow, in: Isotopes and Impurities in Snow and
355 Ice Symposium, edited by: Oeschger, H., Ambach, W., Junge, C. E., Lorius, C., and
356 Serebryanny, L., 118, IASH-AISH Publication, Dorking, 199–203, 1977.
357 Haussener, S., Gergely, M., Schneebeli, M., and Steinfeld, A.: Determination of the
358 macroscopic optical properties of snow based on exact morphology and direct pore-
359 level heat transfer modeling, Journal of Geophysical Research, 117, 1 –20, 2012.
360 Kaempfer, T. U., Schneebeli, M. and Sokratov, S. A.: A microstructural approach to
361 model heat transfer in snow, Geophysical Research Letter, 32, 1-5, 2005.
362 Kaempfer, T. U. and Plapp, M.: Phase-field modeling of dry snow metamorphism,
363 Physical Review E, 79, http://dx.doi.org/10.1103/PhysRevE.79.031502, 2009.
364 Löwe, H., Spiegel, J. K., and Schneebeli, M.: Interfacial and structural relaxations of
365 snow under isothermal conditions, Journal of Glaciology, 57, 499–510, 2011.
366 Löwe, H., Riche, F., and Schneebeli, M.: A general treatment of snow microstructure
367 exemplified by an improved relation for the thermal conductivity, The Cryosphere
368 Discussions, 6, 4673–4693, (2012).
369 Neumann, T. A., Albert, M. R., Lomonaco, R., Engel, C., Courville, Z., and Perron, F.:
370 Experimental determination of snow sublimation rate and stable-isotopic exchange,
371 Annals of Glaciology, 49, 1–6, 2008
372 Neumann, T. A., Albert, M. R., Engel, C., Courville, Z., and Perron, F.: Sublimation
373 rate and the mass-transfer coefficient for snow sublimation, 52, 309-315, 2009.
374 Otsu, N.: A Threshold Selection Method from Gray-Level Histograms, IEEE Transac-
375 tions on Systems Man and Cybernetics, 9, 62–66, 1979.
376 Petrasch, J., Schrader, B., Wyss, P., and Steinfeld, A.: Tomography-based determination
377 of effective thermal conductivity of fluid-saturated reticulate porous ceramics,
378 Journal of Heat Transfer, 130, 1-10, 2008.
379 Pinzer, B. R., and Schneebeli, M.: Snow metamorphism under alternating temperature
380 gradients: Morphology and recrystallization in surface snow, Geophysical Research
381 Letters, 36, 1–4, 2009.
382 Pinzer, B. R., Schneebeli, M., and Kaempfer, T. U.: Vapor flux and recrystallization
383 during dry snow metamorphism under a steady temperature gradient as observed by
384 time-lapse micro-tomography, The Cryosphere, 6, 1141–1155, 2012.
385 Riche, F. and Schneebeli, M.: Thermal conductivity of snow measured by three inde-
386 pendent methods and anisotropy considerations, The Cryosphere, 7, 217–227,
387 (2013).

Schleef, S., Jaggi, M., Löwe, H., and Schneebeli, M.: Instruments and Methods: An improved machine to produce nature-identical snow in the laboratory, Journal of Glaciology, 60, 94–102, 2014.

Stichler, W., Schotterer, U., Frohlich, K., Ginot, P., Kull, C., Gäggeler, H., and Pouyaud, P.: Influence of sublimation on stable isotope records recovered from high-altitude glaciers in the tropical Andes, Journal of Geophysical Research, 106, 22613-22630, 2001.

Sturm, M. and Benson, C.: Vapor transport grain and depth-hoar development in the subarctic snow, Journal of Glaciology, 43, 42-59, 1997.

Sturm, M., and Johnson, J. B.: Natural convection in the subarctic snow cover, Journal of Geophysical Research, 96, 11657–11671, 1991.

Thorpe, A. D. and Mason, B. J.: The evaporation of ice spheres and ice crystals, British Journal of Applied Physics, 17, 541-548, 1966.

Waddington, E. D., Cunningham, J., and Harder, S. L.: The effects of snow ventilation on chemical concentrations, in: Chemical Exchange Between the Atmosphere and Polar Snow, edited by: Wolff, E. W. and Bales, R. C., NATO ASI Series, 43, Springer, Berlin, 403–452, 1996.

Wang, X. and Baker, I.: Evolution of the specific surface area of snow during high-temperature gradient metamorphism, Journal of Geophysical Research Atmosphere., 119, 13690–13703, 2014

Zermatten, E., M. Schneebeli, H. Arakawa, and A. Steinfeld: Tomography-based determination of porosity, specific area and permeability of snow and comparison with measurements, Cold Regions Science and Technology, 97, 33–40, 2014, doi:10.1016/j.coldregions.2013.09.013.

414 **Table 1:** Morphological and flow characteristics of the experiments: Volume flow (V),
415 initial superficial velocity in snow ($u_{D,0}$), initial snow density (ρ_0), initial porosity (ε_0),
416 specific surface area (SSA_0), initial mean pore size (d_{mean}), average inlet ($T_{in,ave}$) and
417 outlet temperature ($T_{out,ave}$), and the average temperature gradient (∇T_{ave}), corresponding
418 Reynolds number (Re) and Peclet number (Pe).
419

Name	V liter min^{-1}	$u_{D,0}$ m s^{-1}	ρ_0 kg m^{-3}	ε_0 –	SSA_0 m^2 kg^{-1}	d_{mean} mm	$T_{in,ave}$ °C	$T_{out,ave}$ °C	∇T_{ave} K m^{-1}	Re –	Pe –
ota1	–	–	284.3	0.69	25.0	0.30	-13.8	-12.5	43.3	–	–
ota2	0.3	0.004	256.8	0.72	26.3	0.33	-14.0	-12.5	50.0	0.07	0.05
ota3	1.0	0.012	256.8	0.72	24.3	0.34	-13.8	-12.3	43.3	0.25	0.19
ota4	3.0	0.036	265.9	0.71	21.7	0.36	-14.6	-13.0	53.3	0.78	0.61

420
421
422
423 **Table 2:** Estimated sublimation rate S_m using the mass transfer coefficient h_m deter-
424 mined by Neumann et al. (2009) and the corresponding average surface area per volume
425 $SA_{V,ave}$. S_m can be compared with the measured sublimation rate of the experiment $S_{m,exp}$
426 (Eq. (1)).
427

Name	$SA_{V,ave}$ mm^{-1}	h_m m s^{-1}	S_m kg m^{-3} s^{-1}	$S_{m,exp}$ kg m^{-3} s^{-1}
ota1	22.44	$0.75 \cdot 10^{-4}$	$4.83 \cdot 10^{-4}$	$0.68 \cdot 10^{-6}$
ota2	23.98	$1.15 \cdot 10^{-4}$	$2.99 \cdot 10^{-4}$	$4.48 \cdot 10^{-6}$
ota3	21.88	$2.17 \cdot 10^{-4}$	$5.15 \cdot 10^{-4}$	$0.76 \cdot 10^{-6}$
ota4	19.61	$5.16 \cdot 10^{-4}$	$10.9 \cdot 10^{-4}$	$0.08 \cdot 10^{-6}$

428

Figure captions

Fig. 1. Schematic of the ice-air interface transport processes: a) Under isothermal conditions Kelvin-effect leads to a saturation of the pore space in the snow but did not affect the structural change (Ebner et al., 2015a); b) Air cooling by a negative temperature gradient along the flow direction leads to a change in the microstructure due to deposition (Ebner et al., 2015b); c) Air warming by a positive temperature gradient along the flow has a negligible total mass change of the ice but a strong reposition effect of water molecules on the ice grains, shown in this paper.

Fig. 2. Evolution of the 3-D structure of the ice matrix with applied temperature gradient and advective conditions. Experimental conditions (from left to right) at different measurement times from beginning to the end (top to bottom) of the experiment. The shown cubes are 110 × 40 × 110 voxels (2 × 0.7 × 2 mm^3) large with 18 μm voxel size (a high resolution figure can be found in supplementary material).

Fig. 3. Superposition of vertical cross-section parallel to the flow direction at time 0 and 108 hours for 'ota3' (left panel) and 'ota4' (right panel). Sublimation and deposition of water vapor on the ice grains were visible with an uncertainty of 6 % (a high resolution figure can be found in supplementary material).

Fig. 4. Temporal evolution of a) the mean pore size, d_{mean}, of the snow samples obtained by an opening-size distribution, b) the porosity, ε, obtained by triangulated structure surface method, c) the specific surface area, SSA, of the ice matrix obtained by triangulated structure surface method, and d) the effective thermal conductivity of the snow sample, k_{cond}, estimated by DPLS simulations. The sizes of the volumes used for the computation of each property are 350 × 350 × 350 voxels (6.3 × 6.3 × 6.3 mm^3).

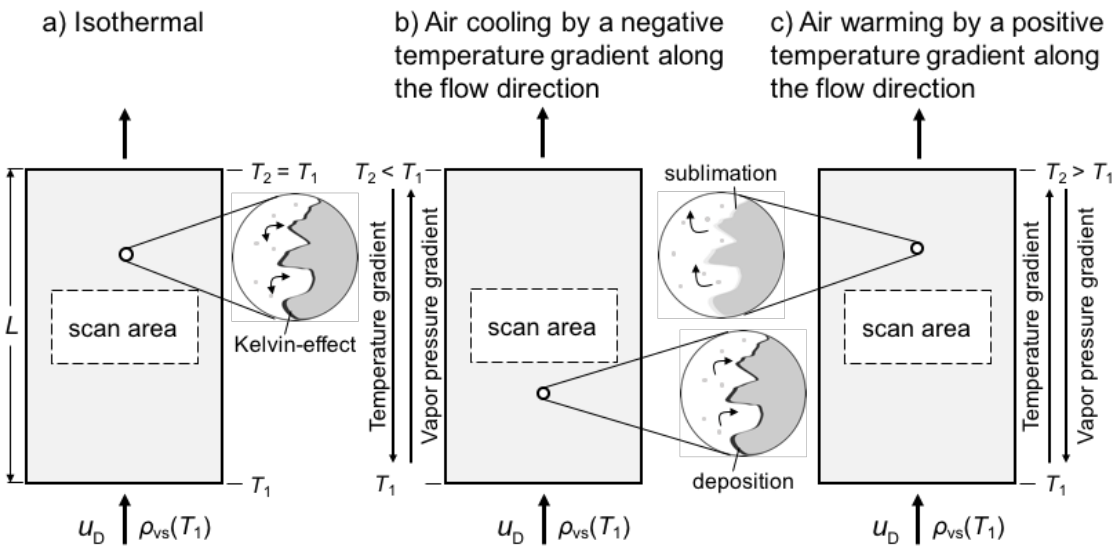

457

458 **Fig. 1**

459

460

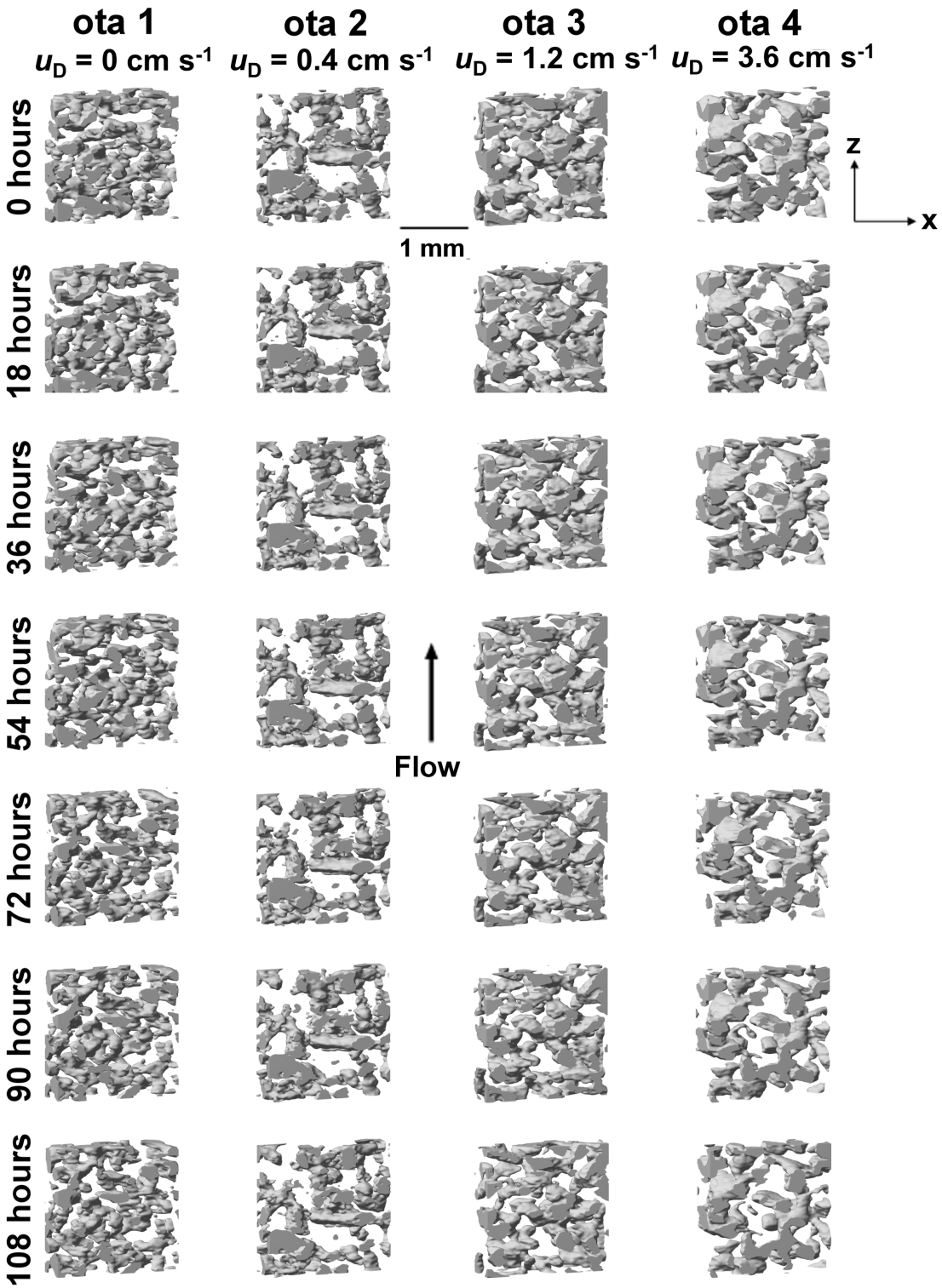

461

462 **Fig. 2**

463

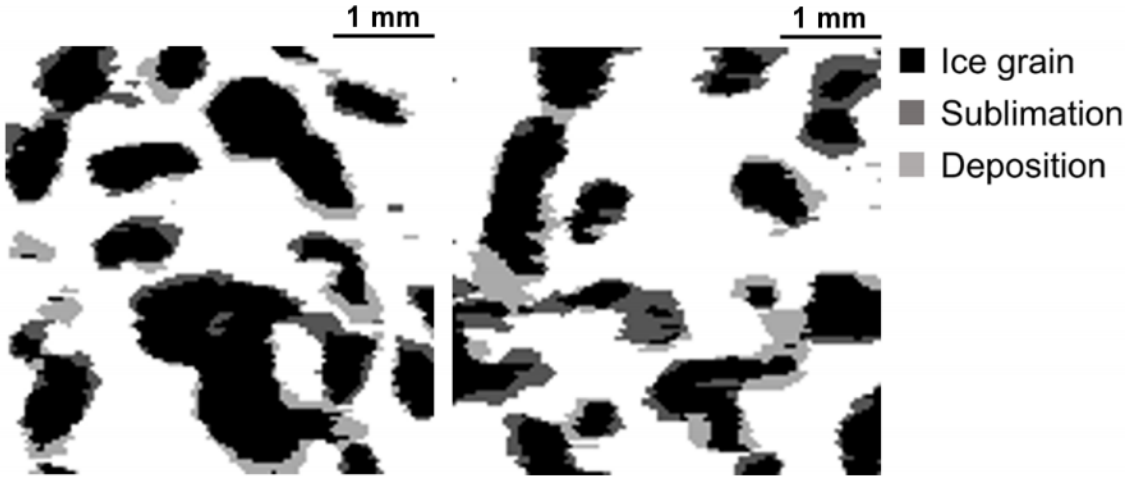

Fig. 3

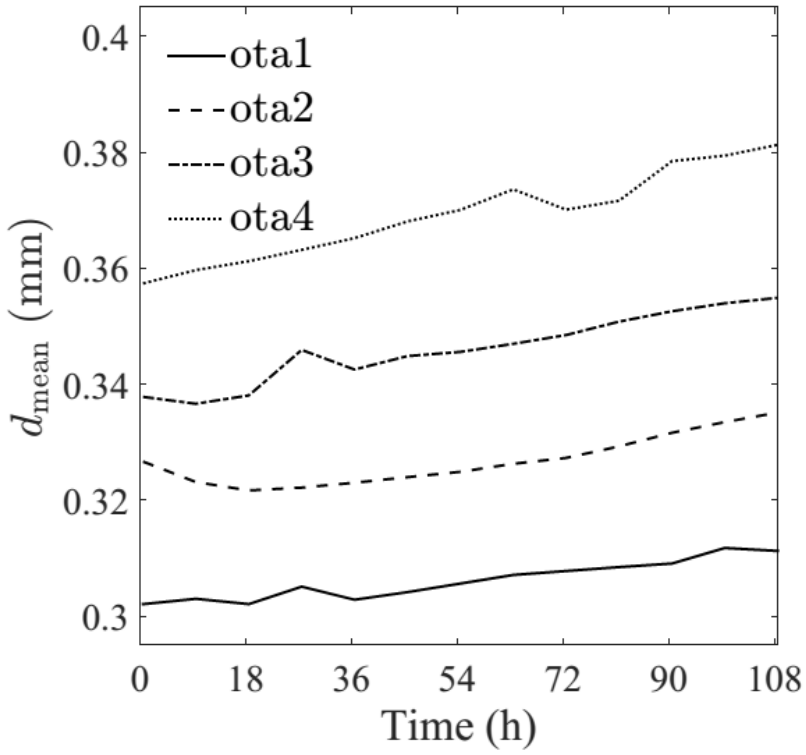
ota1
ota2
ota3
ota4
0.4
0.38
0.36
0.34
0.32
0.3
d_{mean} (mm)
0
18
36
54
72
90
108
Time (h)

Fig. 4 a)

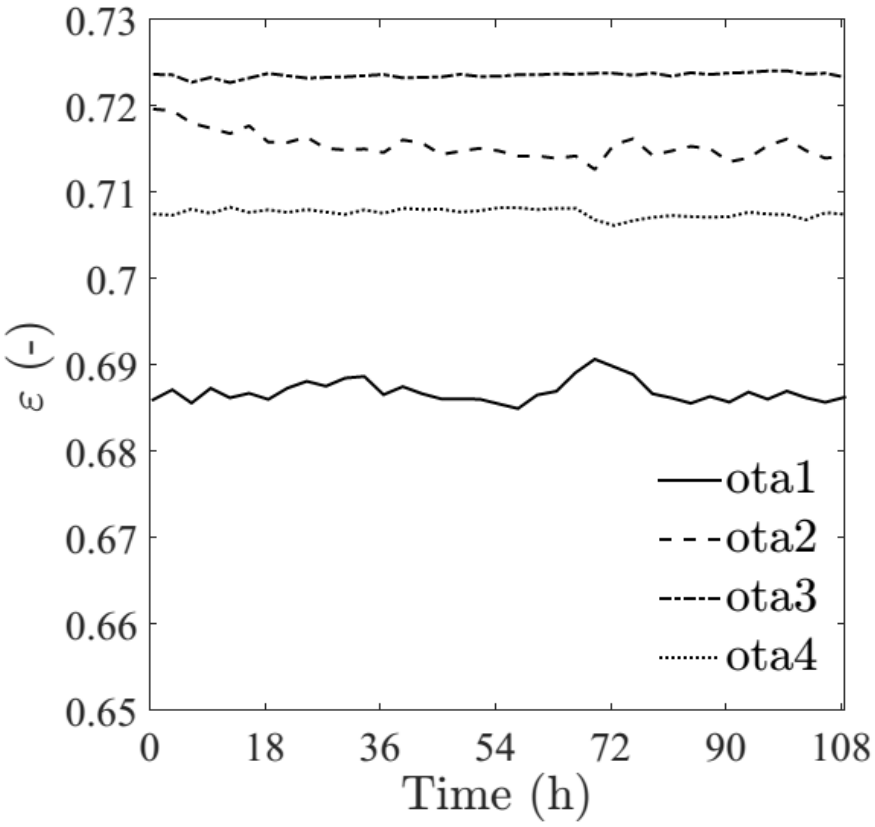

471

472 **Fig. 4 b)**

473

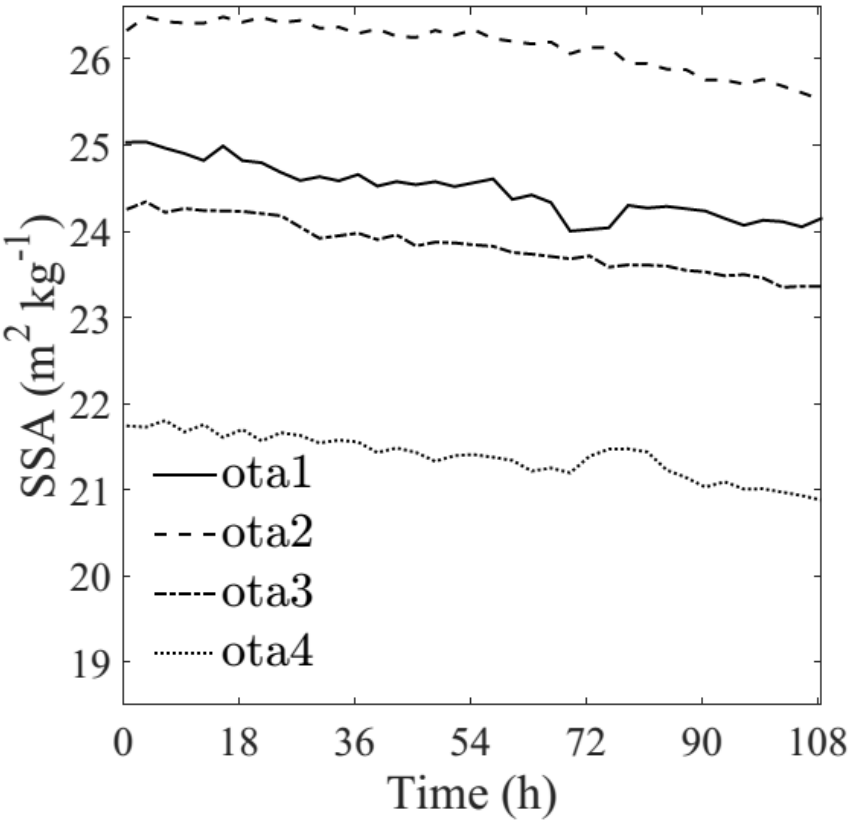
SSA (m^2 kg^{-1})
Time (h)
ota1
ota2
ota3
ota4
26
25
24
23
22
21
20
19
0
18
36
54
72
90
108

Fig. 4 c)

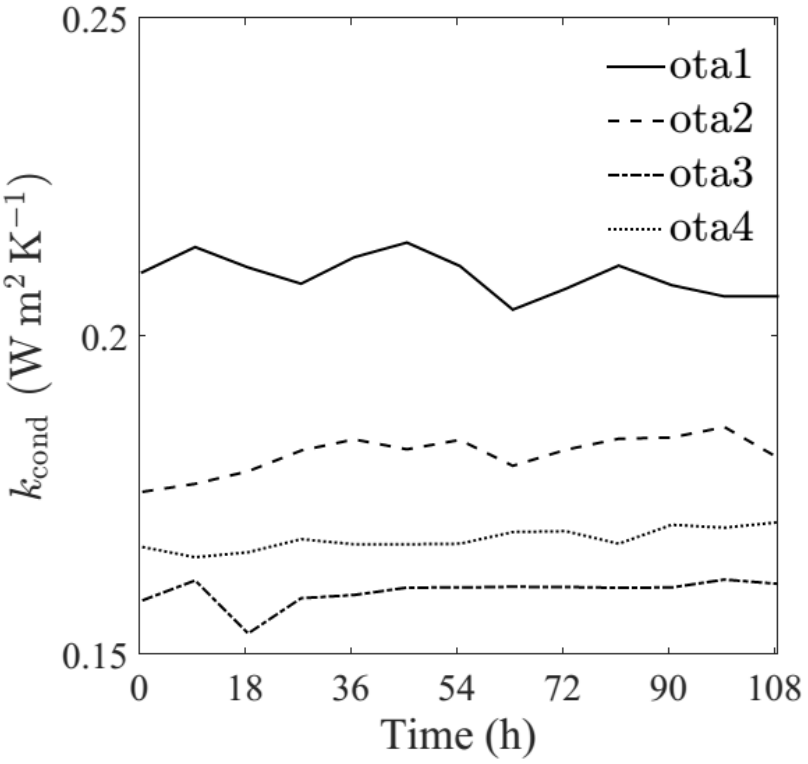

477

478 **Fig. 4 d)**